Thin–Walled Structures 205 (2024) 112379

Contents lists available at ScienceDirect

Thin-Walled Structures

journal homepage: www.elsevier.com/locate/tws

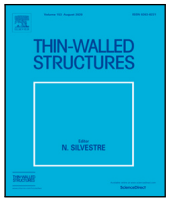

Full length article

Experimental investigation and probabilistic analysis of the buckling load of isotropic cylinders under multiaxial loading

Niklas Reuter [a,*], Stefan Panek [b], Benedikt Kriegesmann [a], Georgios Balokas [a], Tobias S. Hartwich [b], Dieter Krause [b]

[a] Hamburg University of Technology, Institute for Structural Mechanics in Lightweight Design, Hamburg, Germany
[b] Hamburg University of Technology, Institute of Product Development and Mechanical Engineering Design, Hamburg, Germany

ARTICLE INFO

Dataset link: https://doi.org/10.15480/882.13221

Keywords:
Probabilistic design
Buckling
Imperfection sensitivity
Cylindrical shells

ABSTRACT

This paper presents a multitude of experimental results for cylindrical shells under combined loading. The loading is a combination of axial compression and bending moment. These are accompanied with numerical simulations. The load ratio itself is subject to scatter, a direct comparison and application of results for the sizing of shells is not straight forward. Therefore, a new approach is presented, which transfers the results to normalized load factors.

1. Introduction

Thin-walled cylindrical shells can be found as structural elements in various fields of application, such as aerospace and civil engineering. Under certain load types, such as axial compression, torsion, bending or hydrostatic pressure, these shells are prone to structural failure by buckling. The load carrying capacity in these cases, commonly referred to as buckling load, is known to be sensitive to a number of different influencing factors [1]. The buckling behavior of cylindrical shells under axial compression load and the different potentially occurring influencing factors have been intensely studied subjects for the last century. Several works summarize the extensive theoretical and experimental history of this research, such as [2–5].

Even though in practice the different critical buckling load cases frequently occur in varying in combinations, a topic that has gained comparatively little attention is the buckling of cylindrical shells under combined loading. Winterstetter and Schmidt [6] compiled a number of experiments, mostly on metallic shells, in which axial compression was combined with hydrostatic pressure, axial compression with a torsional moment or external pressure with torsion. The results exhibit a strong scatter with qualitatively different interaction curves of the buckling load between load combinations. The majority of publications that consider combined loading investigate the combination of axial compression and internal pressure, e.g., [7–10]. There are also some experimental studies regarding axial compression and torsion with isotropic shells, e.g., [11,12] and more recently with CFRP shells, e.g., [13–15]. With regards to bending as buckling inducing load only very few publications on test campaigns exist, e.g., [16,17]. However, these studies only consider pure bending. So far, only one experimental study conducted by Bruhn [12] is known to analyze buckling of cylindrical shells in multiaxial load cases consisting of combined compression, torsion and bending. In this campaign, a total of 29 cylinders with varying length and R/t-ratio made from thin celluloid sheets were tested in a setup manually operated via wire-pulley-lever systems [12].

The design of buckling critical cylindrical shell structures for combinations of different load types is considered in the widely accepted design guideline NASA SP-8007 [1] and specifically for steel shells in the European Standard EN 1993-1-6, also referred by the title Eurocode 3 [18]. Both of these design guidelines were originally established to provide a lower bound of buckling loads for metallic cylinders, even though the NASA SP-8007 was later revised to also include orthotropic materials as well as stiffened shells [1]. Interaction between different co-occurring load types is considered to varying degrees by the two approaches. While the NASA SP-8007 assumes a strictly linear interaction between any number of simultaneously acting buckling inducing loads [1], Eurocode 3 considers a linear or non-linear interaction depending on whether axial compression is combined with bending or axial compression with torsion [18] (see Fig. 1). Both guidelines explicitly state that the underlying assumptions for these interaction curves may lead to overly conservative designs and refer

* Corresponding author.
E-mail address: niklas.reuter@tuhh.de (N. Reuter).

https://doi.org/10.1016/j.tws.2024.112379
Received 29 April 2024; Received in revised form 19 August 2024; Accepted 23 August 2024
Available online 30 August 2024

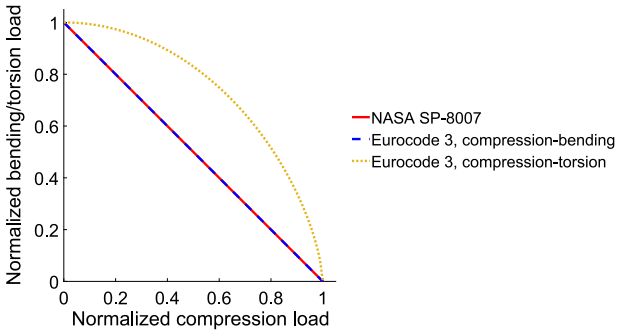

Fig. 1. Ratio of acting load and allowable load for axial compression and bending or axial compression and torsion according to NASA SP-8007 [1] and Eurocode 3 [18].

to the lack of experimental data required to improve the precision of such approaches [1,18].

Thus, the purpose of this contribution is to significantly augment the database on buckling experiments with cylindrical shells in multiaxial load cases. This paper presents the results of an experimental study in which a set of 22 nominally identical isotropic polymer cylinders is tested under different load combinations of bending and axial compression induced by eccentric load introduction. In addition, a set of seven nominally identical steel cylinders is tested under combined bending and axial compression in a test rig allowing for simultaneous application of tilting and centric compression. The resulting buckling load distributions are discussed and a normalized load factor for comparing buckling loads in multiaxial load cases is introduced. Numerical models are implemented based on the experimental results and the accuracy of the numerical buckling load predictions is analyzed. Finally, based on the larger amount of data available, probabilistic Monte Carlo analyses are carried out for the polymer shells to analyze the influences of different scattering parameters such as geometric imperfections or wall thickness.

2. Buckling load factor λ

When considering combined loading, the maximum load reached can be best expressed by a load factor that scales the different loading components. An obvious choice for such a load factor when considering a combination of axial load and bending moment is given by

$$\lambda = \sqrt{\left(\frac{BL}{BL_{perf}}\right)^2 + \left(\frac{BM}{BM_{perf}}\right)^2} \tag{1}$$

Here, BL and BM are the buckling load and buckling moment of one instance (e.g. observed in an experiment), and BL_{perf} and BM_{perf} are the buckling load and moment of the ideal cylinder without imperfections (obtained from numeric simulation). This definition of a load factor has a big disadvantage for the comparison of experimental tests and simulation conducted in this paper. The reason is that a deviation of the nominal combination of force and moment also leads to a different load factor. Hence, a deviation of load factors does not allow to conclude whether the achieved load level differs or only a different combination of force and moment is obtained. Therefore, the expanded definition of a load factor λ as given in Eq. (2) is used in the following.

$$\lambda = \frac{\sqrt{BL^2 + BM^2}}{\sqrt{BL_{perf}^2 + BM_{perf}^2}} \cdot cos\left(tan^{-1}\left(\frac{BM}{BL}\right) - tan^{-1}\left(\frac{BM_{perf}}{BL_{perf}}\right)\right) \tag{2}$$

The load factor λ therefore projects the vector which is spanned by the measured buckling moment and buckling load onto the vector pair of the analytically calculated perfect buckling load (see Fig. 2). The perfect buckling load is determined by a linear eigenvalue analysis of a perfect shell with initial geometry. Pure axial compression load would therefore yield a result on the x-axis, while pure bending load gives a result located directly on the y-axis.

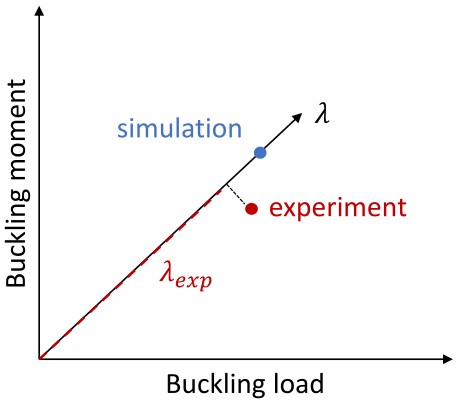

Fig. 2. Load factor λ.

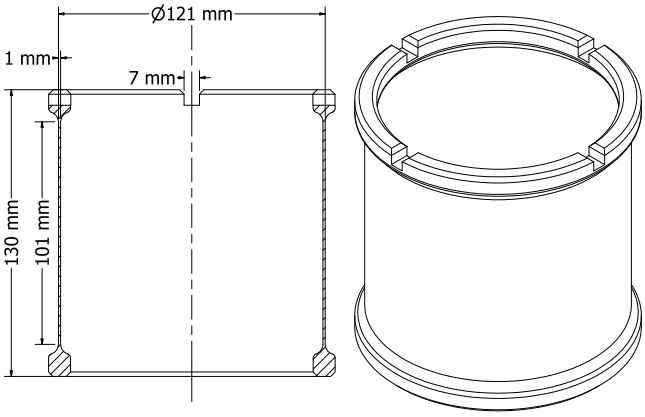

Fig. 3. Sketch of the printed polymer cylinder.

3. Experimental setup

In this section, the experimental setup for each of the two test series is described. The first one considers 22 polymer shells, whereas the second one deals with seven steel shells, sequentially labeled Z1S4 to Z7S4.

3.1. Test setup for polymer cylinders

The polymer cylinders, as schematically shown in Fig. 3, are manufactured using the 3D printer Form 2 by Formlabs. The nominal dimensions are summarized in Table 1. One advantage of additive manufacturing of the shells is that it allows to integrate the test specimen and load introduction structure, namely the much thicker end rings, into one singular component as opposed to commonly used additional clamping elements. The material was characterized to be isotropic [19]. The material properties likely differ from the nominal ones given in the data sheet, as several aspects (e.g. print orientation, print settings) are known to influence the properties.

The buckling tests with polymer cylinders were carried out on a universal testing machine with a modified clamping device. The shells were fixed at the lower edge in a metallic clamping device which restricts all translational degrees of freedom as well as rotation of the shell about its axis. The axial force was applied as a concentrated load via a pin resting on the upper clamping. In order to generate a multiaxial load case, the force was applied at different, predefined distances (5 mm, 10 mm, 15 mm, 20 mm, 40 mm and 60 mm) from the central axis of the cylinder via a steel plate as shown on the right side in Fig. 4. The resulting load case is schematically visualized in Fig. 4 on the left.

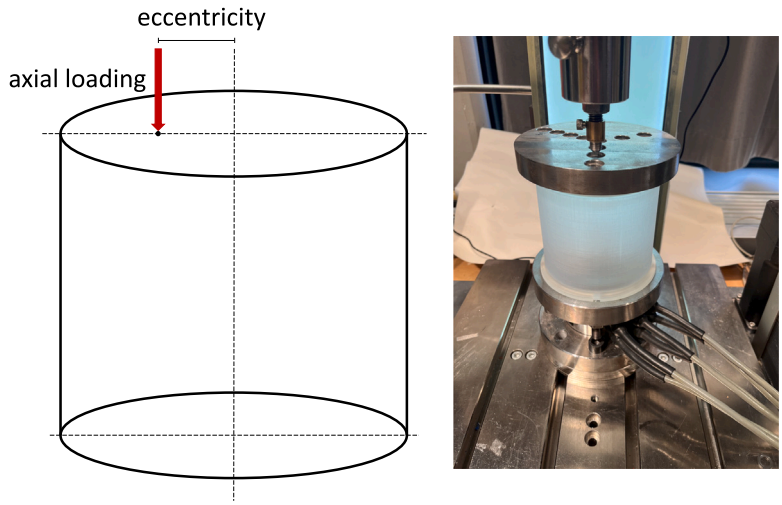

Fig. 4. Sketch of the load case (left) and experimental setup with a polymer cylinder (right).

Due to the eccentric load introduction, a bending moment acts on the shell in addition to the axial load, which is measured at the lower clamping. In order to record the occurring forces and moments, a multi-component transducer from Gassmann Theiss Messtechnik GmbH was installed. This load cell can record forces and moments in all spatial directions. The cylinders were tested until buckling occurred, which is characterized by a sudden, significant drop in load. As the cylinders buckled in the elastic range, each shell could be tested several times. The tests were carried out in random order and with variation of the direction of eccentric load application for each shell. Between any two tests with the same specimen a minimum of 10 min was waited to ensure that the cylinder recovered to its initial shape. Comparing the first test of one cylinder and a test after several experiments, no difference in the stiffness was obtained. Therefore, effects like the Mullins effect can be neglected. In addition, relative slenderness values are calculated following Eurocode 3 [18] to check for potential plasticity. The relative slenderness of the considered shells is 2.38 whereas the plastic limit relative slenderness amounts to 0.96, thus supporting the assumption of pure elastic buckling. Therefore, any plastic behavior of the polymer material is neglected.

An eccentricity of 60 mm is equal to the radius of the cylinder. Therefore, in this case, the load introduction is directly aligned with the shell wall. The results of all tests performed with this eccentricity significantly differed from all other tests with lower eccentricities, yielding much lower buckling loads likely due to the additional influence of local load introduction directly at the shell edge. Hence, the data from these experiments are not further discussed in this publication.

With the given experimental setup, it is not possible to achieve arbitrary combinations of force and moment, because the moment results from the eccentric axial load introduction. Therefore, neither a load case with pure bending nor a load case with an arbitrary ratio of axial load and moment is achievable. Pure axial loading is possible to achieve by applying the load introduction in the center of the shell which, due to imperfections, also results in a small bending moment that has been measured.

3.2. Test setup for steel cylinders

In addition to the previously described polymer shells, a set of seven nominally identical steel shells is investigated. These shells are made from 0.5 mm thick steel sheets that are rolled into the desired shape and face welded. To minimize a potential stiffening influence, the welds are machined down to be of equal thickness as the shell wall. The nominal specifications of the investigated shells are given in Table 1.

Table 1
Nominal specifications of investigated shells.

Designation	Polymer cylinders	Z1S4 - Z7S4
Inside radius [mm]	59.5	114.0
Total length [mm]	130.0	255.0
Free length [mm]	100.0	215.0
Nominal R/t ratio	60	228
Material	Resin	Steel

Elastic tests as well as buckling experiments are carried out on the Hexapod test rig at TUHH, a servohydraulic platform that is able to move in six degrees of freedom [20]. The test setup for these experiments is based on the one extensively described in [21]. Both edges of the shells are held in steel fixtures with an epoxy potting as introduced by [22], resulting in fully clamped shell boundary conditions. The test rig boundary conditions can also be considered fully clamped, as the lower steel fixture is mounted on a 6-DoF load cell while the upper clamping is attached to the platform of the test rig via screws, as illustrated in Fig. 5. Mounting and fixating the test specimen in the test rig is done in a force-free manner, achieved by careful adjustment of the test platform to counter the buildup of forces and moments during the attachment process.

In addition to the internal sensors of the test rig tracking all translational and rotational movements, three optical displacement sensors are set up along the circumference of the shells, allowing to measure the tilting and axial displacement of the upper shell edge. Furthermore, three axially aligned strain gauges are applied to the shell, measuring the local strains along the circumference. Finally, an ARAMIS-System for digital image correlation (DIC) is positioned to record the side of the shells where, due to the combination of bending and compression, the maximum stresses are expected.

Loads are applied to the shells by lowering the platform, as well as rotating the platform about the mid-point of the shells. This way it is possible to apply bending moments with minimal load imperfections, as opposed to combined bending and shear loads when just tilting one of the shell edges. All shells are positioned in the test rig such that the weld is aligned with the positive Y-axis and bending loads are applied by negative rotation of the test platform about the Y-axis. This way, any possible influence of the welds on the test results is minimized.

4. Imperfection measurement

The following sections describe the different types of imperfections that were considered and measured within this study which may influence the buckling loads of the investigated shells.

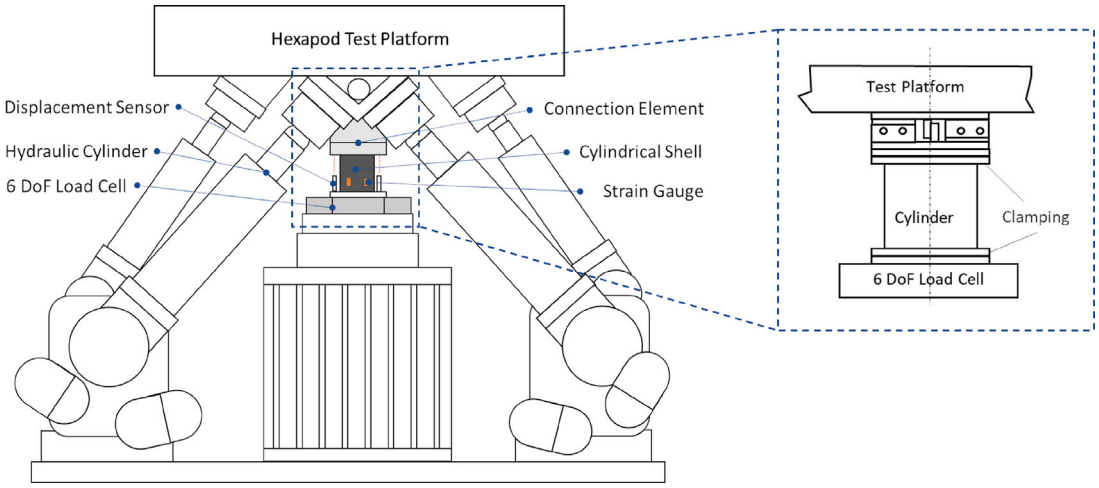

Fig. 5. Schematic visualization of test set-up in the Hexapod test rig based on [21].

4.1. Geometric imperfections

The geometric imperfections of all investigated shells are measured with the photogrammetric system ATOS by GOM. The system was used to measure the outer surface of the cylinders. Due to the integrated load introduction structure, the inside surface of the polymer cylinders could be measured as well. From this data, the actual geometry and thickness is determined and the geometric imperfection can be calculated. The geometric imperfections are radial deviations of the mid surface from the initial geometry of a perfect cylinder. A common approach to represent geometric imperfections of cylindrical shells is the use of half-wave cosine Fourier series (see, e.g., [23–25]).[1], given by

$$\overline{W}(x,y) = 2t \sum_{k=0}^{n_1} \sum_{l=0}^{n_2} cos\frac{k\pi x}{L}\left(A_{kl} cos\frac{ly}{R} + B_{kl} sin\frac{ly}{R}\right) \tag{3}$$

Herein the geometric imperfections are characterized by the Fourier coefficients (FC) A_{kl} and B_{kl}. In Eq. (3), R, L, and t are the radius, length and thickness of the cylinder. For the polymer cylinders, the upper bounds of the sums are chosen to $n_1 = 39$ and $n_2 = 19$. Hence, $40 \times 20 = 800$ FC are used to represent the imperfections, which is much less data compared to the 9180 nodes with 3 coordinates, which are obtained from measurements. In case of the steel shells, the same general procedure is followed. Due to the larger dimensions and expected higher imperfection sensitivity, these shells are represented by 91×53 Fourier coefficients. The FC are assembled in the random vector $\mathbf{Y}$, with the covariance matrix $\boldsymbol{\Sigma}_\mathbf{Y}$ and a mean vector $\boldsymbol{\mu}_\mathbf{Y}$. Thereby, a random realization of imperfections can be generated using Eq. (4).

$$\mathbf{y} = \boldsymbol{\Sigma}_\mathbf{y}^{\frac{1}{2}} \mathbf{z} + \boldsymbol{\mu}_\mathbf{y} \tag{4}$$

The random vector $\mathbf{Z}$ contains uncorrelated entries with a mean of zero and the identity matrix as covariance matrix. For the cylinders considered, a Kolmogorov–Smirnov test was performed for each entry of $\mathbf{Y}$, i.e. for each FC, showing that Gaussian distribution describes the stochastic distribution of the FCs well. When the entries of $\mathbf{Y}$ are Gaussian, then the entries of $\mathbf{Z}$ are not only uncorrelated, but independent.

Fig. 6 on the left shows the measured polymer cylinder (C0607) with radial imperfections scaled by 50. For the resolution of the cylinder mesh, in circumferential direction there is a node at every degree, and in axial direction there is a node every millimeter. The cylinder therefore has 101×360 nodes. The representation in FC is an approximation of the geometry. In Fig. 6 on the right the cylinder is plotted after the transformation with 20×40 FC. The Fourier coefficients of all polymer cylinders considered are published on https://doi.org/10.15480/882.13221.

The polymer cylinders have reoccurring imperfections, namely the one at the top of the cylinders. This imperfection can be related to the manufacturing, in this case the 3D printing process. Fig. 7 shows the measured cylinder geometry as an example, where the reoccurring imperfection is visible again. The remaining 20 cylinders are visualized in Appendix A.2.

In contrast to the polymer shells, all steel cylinders exhibit the most notable geometric imperfection at the weld, as is common for metallic shells. The wind up patterns of these imperfections for two of the investigated shells are shown in Fig. 8 with x indicating the axial coordinate and y as the circumferential one. Here, a significant discontinuity in circumferential direction can be observed which in some cases also shows local buckles in axial direction, e.g. as visualized in shell Z5S4 on the right side of Fig. 8.

4.2. Thickness imperfections

The thickness of the polymer cylinders at each node is determined by calculating the difference of the outer and inner shell. A differing thickness from the initial thickness on the nodes of the cylinder can be treated as a radial geometric imperfection like in the previous section. The workflow to generate Fourier coefficients and random thickness on each node is the same as for the radial geometric imperfection. While the polymer shells do exhibit a notable scatter of wall thickness within each shell, no such variation of thickness can be found in the steel cylinders. Consequently, for those shells a constant wall thickness is assumed and implemented in the numerical models.

4.3. Imperfect load introduction

In experiments, several types of loading imperfections may occur that potentially influence the buckling load [26]. On the Hexapod, shear forces and bending moments in cardinal directions as well as torque on the shells are measured during each test. Although bending was applied displacement controlled strictly about the Y-axis, in several tests significant moments about the X-axis were observed as well. Furthermore, in some buckling tests shear forces up to 5.7% of the axial buckling load were recorded. Another possible imperfection in this setup is eccentric load introduction due to poor alignment of the shell to the test rig. While this was specifically utilized and measured

[1] Note that in most publications, the factor 2 in Eq. (3) is not used. Hence, the Fourier coefficients need to be multiplied by factor 2 when not considering it in the Fourier series.

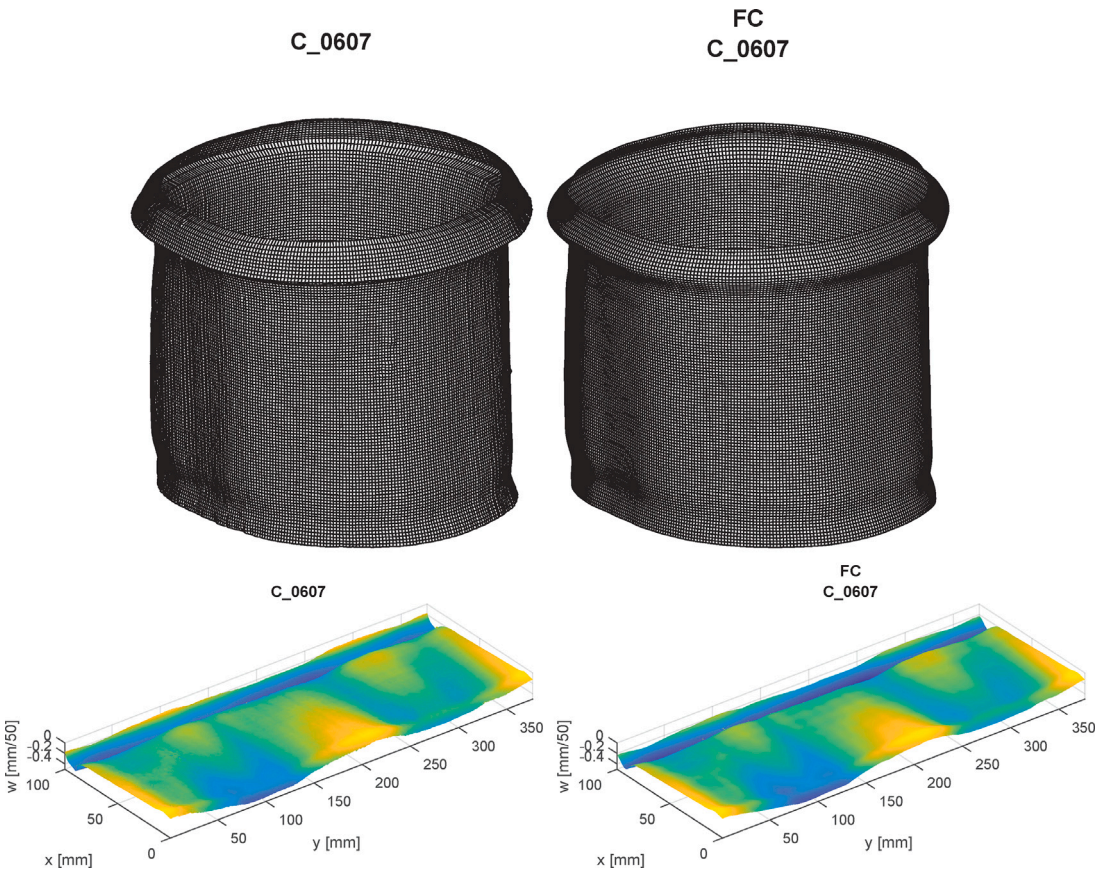

Fig. 6. Measured and plotted data points of cylinder C0607 and FC representation of the same cylinder with a scaling factor of 50, 3D view (top) and unwinded visualization (bottom).

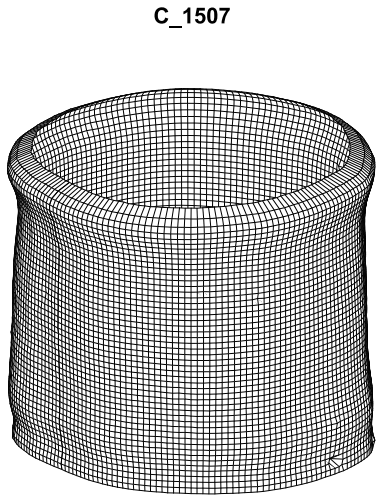

Fig. 7. Measured cylinder geometry of cylinder C1507 with imperfections scaled by the factor 50.

in the test series with the polymer cylinders, the eccentricity could not be precisely determined for the tests on the Hexapod. Hence, an uncertainty of ±1.5 mm for the centric load introduction is estimated, which approximately corresponds to 1% of the shell radius.

Another potential source of inhomogeneous load introduction are imperfections at the shell edges or boundary conditions. In the steel shells, some edge imperfections are present at the welds where the metal sheets were not fully aligned before welding, as shown exemplary in Fig. 9 on the shell Z1S4. These misalignments could not be thoroughly quantified for all of the tested shells and thus are estimated to scatter in height up to 0.5 mm. Local edge imperfections of this type likely lead to locally high stresses and may well result in similar behavior to placing a thin metal shim at the shell edge. The effects of localized edge imperfections have been studied in several publications experimentally and numerically, e.g. [27,28], showing that even a very thin localized shim can lead to a significant decrease in buckling load.

4.4. Scatter of material parameters

To determine the Young's modulus of the polymer cylinders the load–displacement curve of a buckling test can be evaluated. From the linear load–displacement curve (before buckling), the stiffness of the cylinder is calculated with the slope of the curve. The stiffness of the test rig was tested without specimens and has been taken into account. For 21 polymer cylinders,[2] one test with pure axial compression (i.e. no eccentric load introduction) was evaluated. The calculated mean value for the Young's modulus is 1806 MPa with a standard deviation of 255 MPa.

In order to determine Young's modulus and yield stress of the metallic cylinders, tensile tests are carried out with ten coupon specimens according to ISO 6892-1, cut from the same steel sheets that the cylindrical shells are composed of. An excerpt of the stress–strain curves of these tests is given in the right side of Fig. 10. In addition, the stiffness of the tested cylinders in the linear pre-buckling range is taken from load–displacement curves to estimate a smeared axial Young's modulus for the shells themselves. As apparent from the values

[2] In total 22 cylinders where manufactured, but in one case the recorded data are unusable.

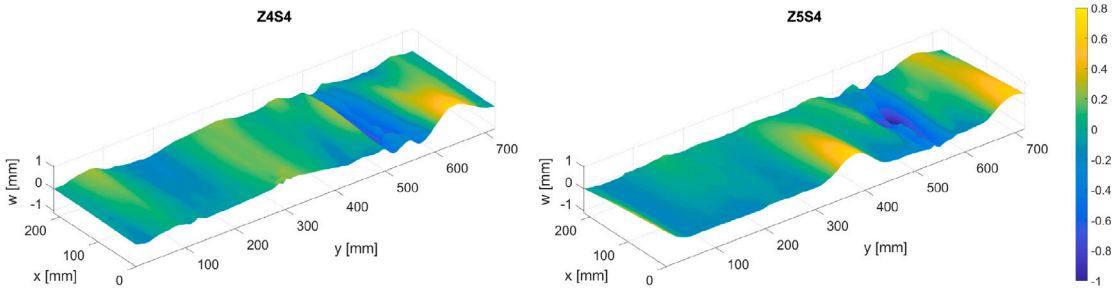

Fig. 8. Wind-up of measured geometric imperfections of steel shells Z4S4 and Z5S4.

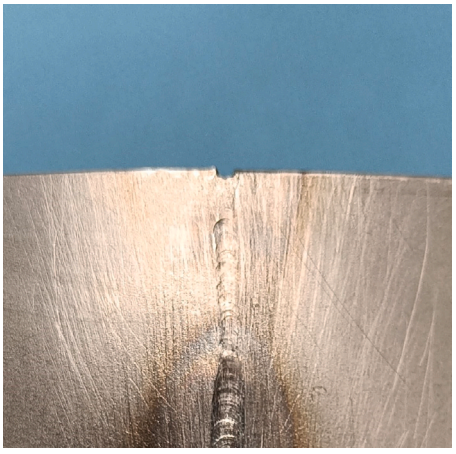

Fig. 9. Edge imperfection at the weld of shell Z1S4.

Table 2
Material parameters gathered from coupon tests.

	Steel coupon test	Steel shells	Polymer shells
Young's modulus [MPa]	108500 ± 5500	128700 ± 8400	1806 ± 255
Yield strength [MPa]	198 ± 7	–	–
Poisson's ratio [–]	0.3	–	–

in Table 2, the calculated stiffness properties differ between the coupon and cylinder specimens. This discrepancy may well be based in part on stabilizing effects of the cylindrical geometry of the tested shells, which does not occur in the coupon tests.

5. Experimental results

In this section the results of the experiments for both sets of cylinders are presented.

5.1. Results of polymer cylinders

The 22 polymer cylinders were tested a total of 519 times with centric and eccentric load introduction. The eccentricity was oriented in four different radial directions (every 90°). The tests were performed in a random order. Normally, the cylinders buckled elastically and therefore were tested several times. However, some cylinders failed during the experiment and therefore could not be tested for every possible eccentricity and orientation. All experimental results are summarized in Fig. 11 and published on https://doi.org/10.15480/882.13221. Every point represents the measured axial load (buckling load) and the measured moment (buckling moment) at which the tested cylinder buckled. The points are grouped together by eccentricity of load introduction. The mean values and standard deviations of buckling load and buckling moment for each eccentricity are listed in Table 3.

In Fig. 12 the load displacement curves of the cylinder C0607 are shown exemplary. For tests with eccentric load introduction, the bending moment is shown on the right axis.

Fig. 13 shows the buckling load as the normalized load factor λ for the different eccentricities. The Figure shows no visible difference within the distribution of λ over the eccentricities. The mean values and standard deviations for each eccentricity are shown in Table 4. The tests with no eccentricity show the lowest mean value and the second highest standard deviation of λ. Despite no moment being introduced during these experiments, in some tests significant bending moments were measured.

One could expect that the ratio of buckling load and buckling moment for a certain eccentricity to be nearly the same for all experiments with the same eccentricity. The moment results from the eccentricity, representing the leverage, and the applied axial load. Even if the load bearing capacity differs between shells, the ratio should stay the same if the eccentricity does not change. However, for all eccentricities a scatter of the ratio is visible.

5.2. Results of steel cylinders

The investigated steel shells exhibit plastic deformation at buckling due to the combination of material properties and comparatively low

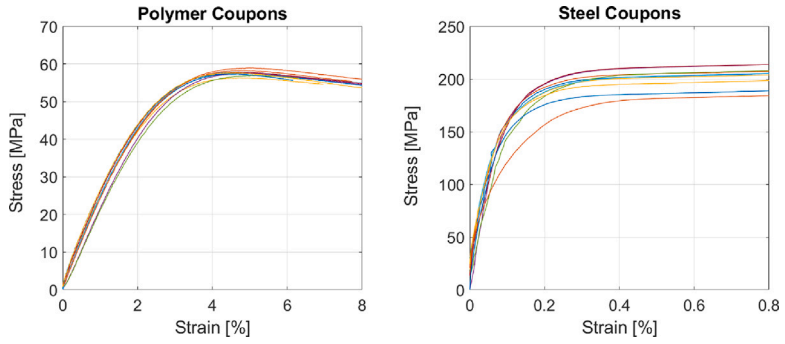

Fig. 10. Stress–strain curves for both materials from tensile tests.

Table 3
Mean values and standard deviation of the buckling load and buckling moment of the experiments.

Eccentricity	Mean value Buckling moment	Standard deviation Buckling moment	Mean value Buckling load	Standard deviation Buckling load
0 mm	6.74 Nm	4.46 Nm	4912 N	905 N
5 mm	20.73 Nm	7.09 Nm	4692 N	773 N
10 mm	32.82 Nm	6.18 Nm	4223 N	748 N
15 mm	42.82 Nm	7.34 Nm	3839 N	631 N
20 mm	49.49 Nm	8.18 Nm	3518 N	582 N
40 mm	66.41 Nm	11.93 Nm	2463 N	417 N

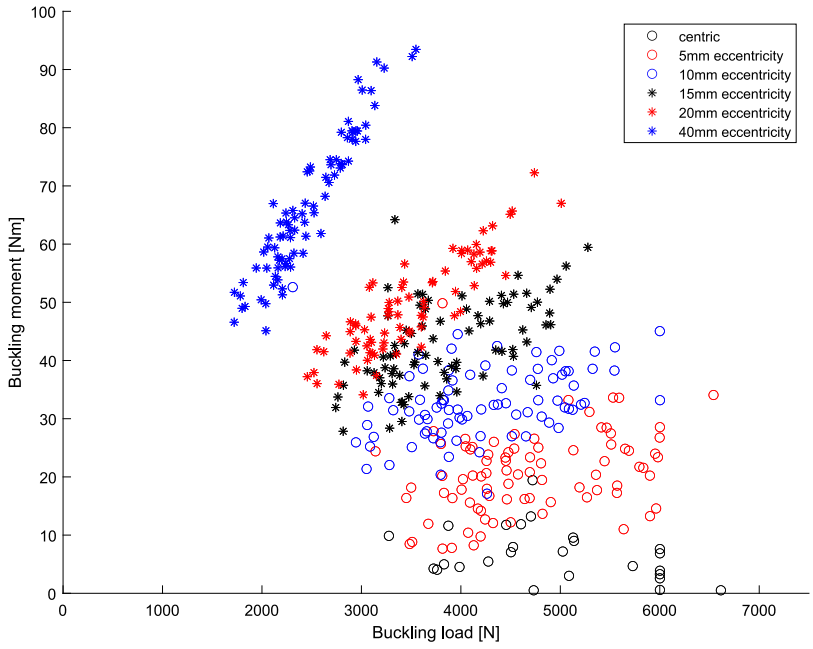

Fig. 11. Buckling load and buckling moment of every experimental for all polymer cylinders.

Table 4
Mean values and standard deviation of the load factor λ of experimental results.

Eccentricity	Mean value λ	Standard deviation λ
0 mm	0.7152	0.1318
5 mm	0.7590	0.1251
10 mm	0.7649	0.1356
15 mm	0.7697	0.1269
20 mm	0.7781	0.1287
40 mm	0.7463	0.1264

R/t-ratio, thus allowing for only one buckling test per cylinder. Consequently, it was attempted to achieve the same ratio between bending moment and compressive force for all shells for better comparability of the results. In order to also allow for some comparability between the two utilized test set ups, the target load ratio was chosen corresponding to the ratio of axial load to bending moment achieved in the tests on polymer shells with an eccentricity of 20 mm. The tests were carried out by pre-loading the cylinders in axial compression with 25 kN, then applying bending and compression simultaneously at constant rates of 0.045 mm/s and 0.01° respectively, until buckling occurred. The switch between the two load steps is visible in the load displacement curves of axial force in Fig. 14. Furthermore, the visualization of bending moments over bending angle for these tests show that particularly shells Z4S4 and Z7S4 reach the maximum bending moment before buckling occurs. Due to the plastic buckling of these shells, no clear snap-through as in Fig. 12 is found. Hence, the onset of buckling is estimated by the point of maximum combined stress acting in the shell. The resulting buckling loads and recorded lateral forces at buckling are given in Table 5 for each shell. Even though the loading procedure was identical for all cylinders, the results exhibit a relatively wide spread in loading ratio similar to the effect observed on the polymer shells. The mean and standard deviation of buckling loads and load deviations are also stated in Table 5. The direction of lateral forces exhibits a volatile scatter, which is in accordance with the common assumption that this value tends to follow a uniform distribution.

Despite bending being applied parallel to the welds in order to minimize their influence, in all tests buckles also formed either on or next to the weld, pointing to the occurrence of loading imperfections in addition to the lateral forces that have not been recorded.

5.3. Comparison of experimental results

The two sets of investigated cylinders differ significantly in material and geometry and consequently achieve buckling loads in widely different load ranges. In order to compare both test series, the experimental buckling loads are normalized with the results of a linear buckling analysis (LBA) for the perfect shells. Due to the variation in load introduction between the test setups, the perfect buckling loads are calculated using separate models for the polymer and steel shells respectively. A more detailed description of the numerical models is given in Section 6. The normalized results of the different types of cylinders are shown in Fig. 15. In this visualization, the relative load carrying capacity of the steel cylinders is generally lower than the one of the polymer cylinders. It is well known that the experimental buckling load decreases relative to the perfect load with increasing R/t-ratio, partially due to increased sensitivity to different influencing factors. Hence, the low normalized buckling load of the steel shells in comparison with the polymer shells is qualitatively in accordance with

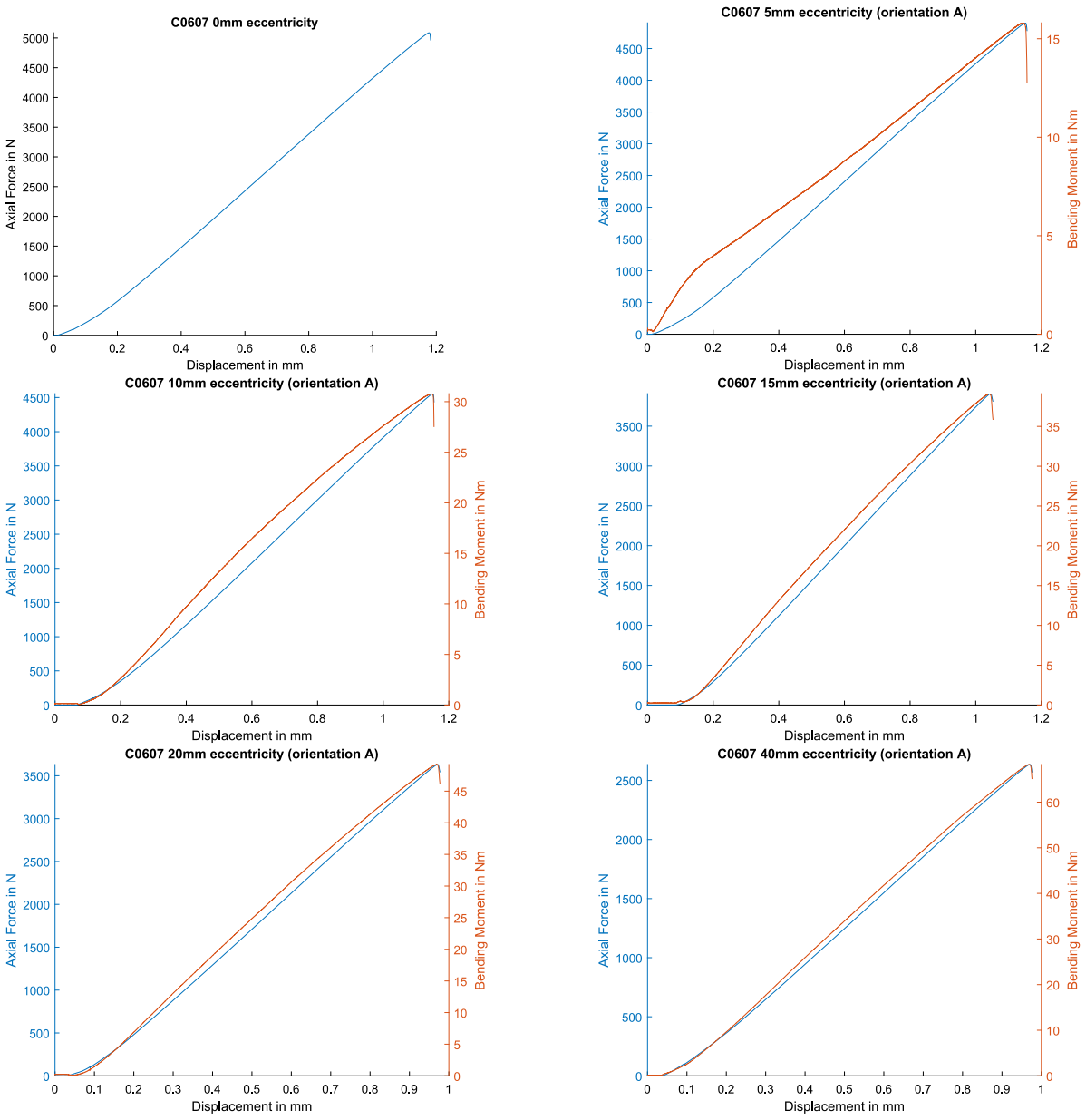

Fig. 12. Load displacement curves for cylinder C0607 for orientation A.

Table 5
Buckling loads of steel cylinders.

	Z1S4	Z2S4	Z3S4	Z4S4	Z5S4	Z6S4	Z7S4	Mean	Standard deviation
Axial load [kN]	41.1	40.0	38.1	40.7	41.1	39.3	37.9	39.7	1.3
Bending moment [kNm]	0.77	0.87	0.82	0.59	0.64	0.60	0.51	0.69	0.13
Lateral force [kN]	2.35	1.03	1.13	0.36	0.40	0.61	1.47	0.94	0.78
Lateral force direction	−173°	82°	−100°	106°	−34°	131°	−136°	−13°	119°

theory. In the investigated cylinders, particularly the misalignment at the welds may greatly contribute to the low buckling loads.

Furthermore, the test results of the steel shells do exhibit a significantly lower scatter than the polymer shells. Calculating the load factor λ for the seven steel shells yields a mean of 0.462 and a standard deviation of 0.026 with respect to the perfect buckling load. However, even though all of these tests were carried out with the goal of achieving the same ratio of bending to compression load, the scatter in resulting load ratios is comparatively large. This may well be a result of differences in the structural bending and compression stiffness between shells.

6. Numerical analyses

For the finite element model of the cylinders, linear four-node shell elements with reduced integration (S4R) and three integration points for the thickness have been used. A mesh convergence study has been conducted, which is described in Appendix A.3. The implemented boundary conditions represent a fixed clamping at bottom of the shells. The top is fixed in the radial directions and allows a translation in the axial direction of the cylinder. In case of the polymer cylinders, an axial load is applied to the shell at the given eccentricity, whereas for

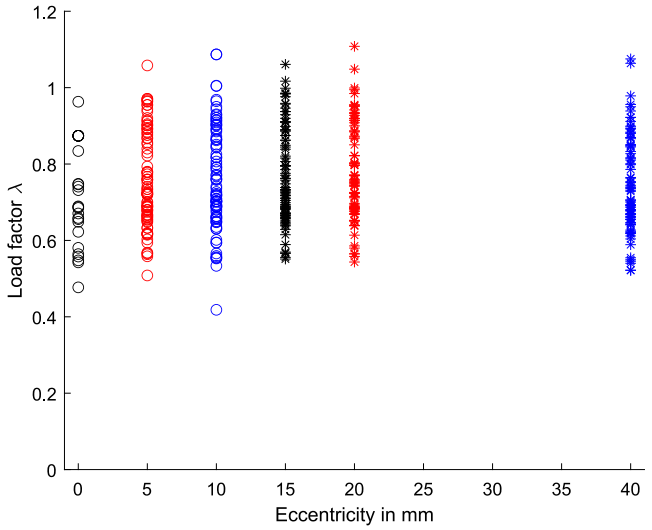

Fig. 13. Load factor λ for the results of experiments with polymer cylinders.

the steel cylinders, axial compression and bending load are introduced on a fixed master node at the midpoint of the shell which is rigidly connected to the upper shell edge. Thus, the numerical models are set up to give an accurate representation of the load introduction that was utilized during each test series. To determine the buckling loads, a geometrically non-linear analysis was performed with the software Abaqus (Version 2024).

Fig. 16 shows experimental results of the polymer cylinders together with Linear Buckling Analysis results using the perfect geometry and the design load/moment according to the NASA SP-8007. As to be expected, the results of the LBA show higher buckling loads than the experiments. The design loads following NASA SP-8007 are within the range of the buckling loads of the experiment. The knockdown factor for axial compression is shown in Eq. (5) and for bending in Eq. (6) with the value of ϕ from Eq. (7). This knockdown factor is used with the analytical estimation of the buckling, using Eqs. (8) for axial compression and Eq. (9) for bending. For the analytical estimation, the nominal thickness ($t = 1$ mm), the radius ($R = 60$ mm), the Young's modulus ($E = 1800$ MPa) and Poisson's ratio ($\nu = 0.3$) are used. The fact that not all experimental results are above the design load shows that NASA SP-8007 is not conservative for the polymer cylinders considered.

$$\gamma_{axial} = 1 - 0.901\left(1 - e^{-\phi}\right) \tag{5}$$

$$\gamma_{bending} = 1 - 0.731\left(1 - e^{-\phi}\right) \tag{6}$$

$$\phi = \frac{1}{16}\sqrt{\frac{R}{t}} \tag{7}$$

$$F_{analytical} = \frac{2\pi Et^2}{\sqrt{3\left(1-\nu^2\right)}} \tag{8}$$

$$M_{analytical} = \frac{\pi^2 Et^2 R}{\sqrt{3\left(1-\nu^2\right)}} \tag{9}$$

6.1. Comparison of simulation and experiment

To compare the results of the simulation with the experiment, the measured geometrical data and the thickness of the cylinder C0607 was used to simulate the buckling load and buckling moment with the model. The four different orientations were used for the eccentric load introduction. The simulated buckling loads and buckling moments are compared in Fig. 17. Table 6 shows the mean values of the results for the different eccentricities. Overall, the experiments yield lower buckling loads but higher buckling moments compared to the simulation of the specific polymer cylinder. Overall, the simulation shows comparable results to the experiments.

Numerical simulations considering geometric and material non-linearities (GMNA) of the steel shells in contrast show generally greater discrepancies. The model is set up as previously described including the measured shell geometry, the measured material properties and the shear forces recorded during testing. The best agreement between test and simulation is achieved for Z7S4 with an overestimation of axial load and bending moment by about 4.7%. On the other hand, for shells Z3S4, Z4S4 and Z5S4 simulations give results that are 25% to 30% higher than the experimental buckling loads. As the edge imperfection that occurred at the weld on most shells is not implemented in the numerical model, its influence is an unquantified uncertainty that may well be the cause of the volatile scatter of simulation results.

6.2. Numerical buckling analyses

For the perfect shell (a cylinder with initial geometry without any imperfections) with initial geometry a linear buckling analysis (LBA) was performed. The linear buckling analysis is an eigenvalue analysis to determine the point of instability. The linear buckling analysis for the polymer cylinders was performed for a load case with pure axial compression and pure bending and load cases with the given eccentricities. To calculate both buckling moment and buckling load for an eccentric load introduction, first the buckling analysis was performed to determine the buckling load and secondly the moment was then calculated with a linear analysis of the observed buckling load. For the shells tested on the Hexapod, the LBA were carried out in a

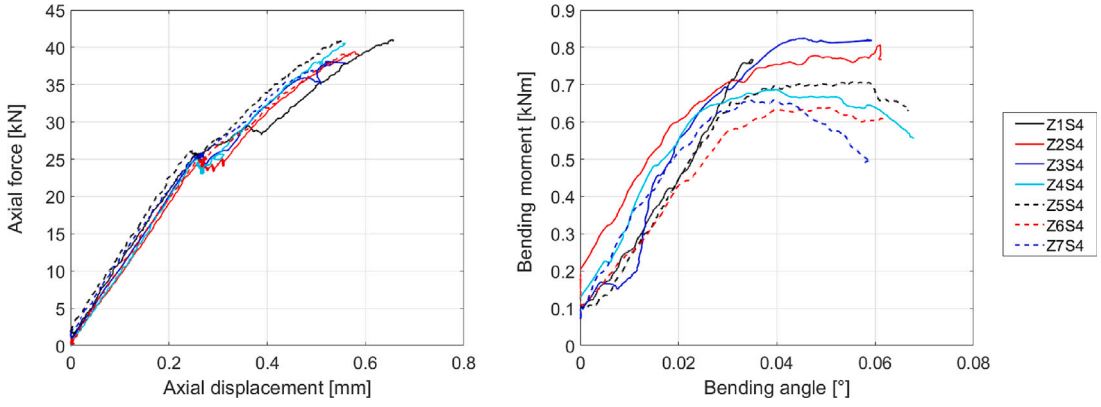

Fig. 14. Load displacement curves for buckling experiments with steel shells.

Table 6
Mean values of buckling loads and buckling moments of simulation and experiment with polymer cylinder C0607.

	0 mm	5 mm	10 mm	15 mm	20 mm	40 mm
Mean buckling load simulation [N]	5558	5099	4500	4062	3696	2703
Mean buckling load experiment [N]	5087	4792	4369	3952	3613	2518
Mean buckling moment simulation [Nm]	0.32	15.32	27.21	36.92	44.86	65.82
Mean buckling moment experiment [Nm]	2.99	18.42	29.14	41.55	49.42	67.38

Table 7
Perfect buckling load and buckling moment of the perfect polymer shell for different eccentricities e.

	Pure bending	Eccentricity e					
		0 mm	5 mm	10 mm	15 mm	20 mm	40 mm
Buckling load [N]	/	6867	6181	5521	4975	4521	3300
Buckling moment [Nm]	240.23	0.00	18.77	33.51	45.23	54.74	70.20

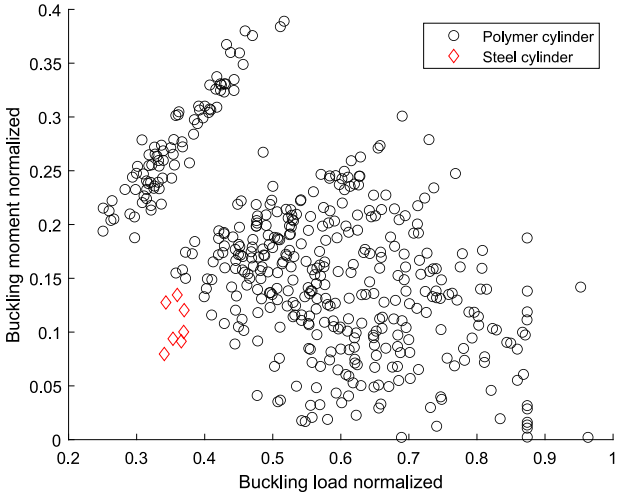

Fig. 15. Normalized results of the two different cylinder types.

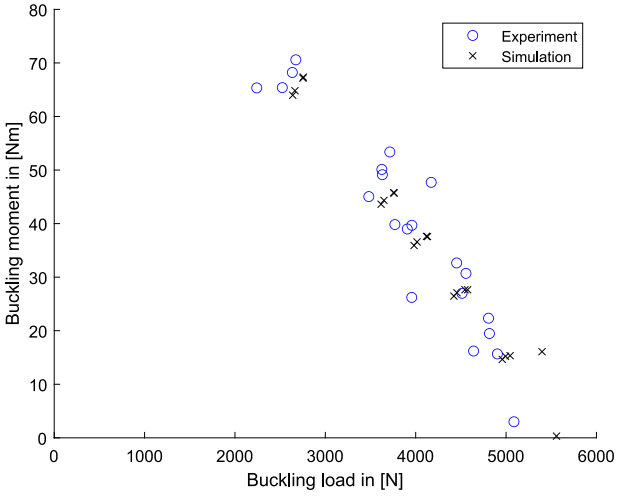

Fig. 17. Results of the experiments and simulations of polymer cylinder C0607 for every eccentricity and every orientation.

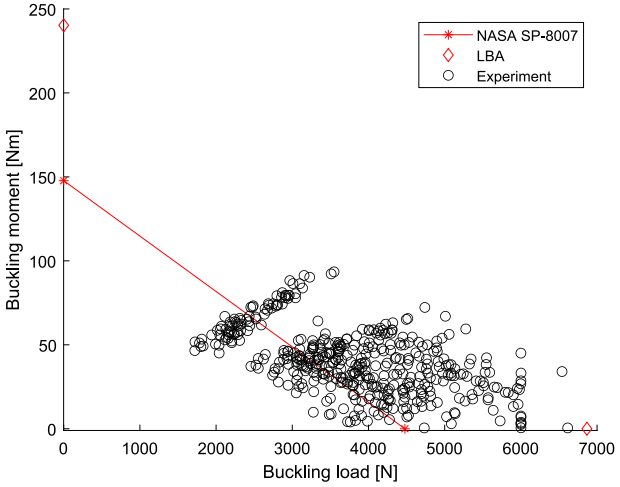

Fig. 16. NASA SP-8007 and Linear Buckling Analysis compared to the experimental results.

singular step using the previously described model, thus allowing to exactly implement the ratios of axial load to bending moment that were observed in experiments.

The results of the simulation of a perfect polymer cylinder is shown in Table 7. These values are used for the normalization of the load factor λ.

The thickness of the shell influences the buckling loads strongly. To show that influence numerically, a buckling analysis of a perfect shell with a thickness 10% below the initial thickness was performed. The first eigenvalue for a pure axial loading is with 5569 N around 18.9% smaller compared to a shell with a thickness of 1 mm. For pure bending, the first eigenvalue is 192.9 N m and is therefore 19.7% smaller.

The nonlinear analysis of imperfect cylinders was performed with a load driven analysis. The buckling loads were determined by observing the maximum load before the analysis aborted. The analysis aborts because the load cannot be increased which is equivalent to buckling. The maximum stresses in the polymer cylinders of approximately 20 MPa are much lower than the yield stresses observed for the same material by Drücker et al. [19]. Comparing to the performed coupon test for the polymer material (see Fig. 10), the calculated stress is much lower than the yield stress, as well. Therefore, plasticity was neglected in the material model for the simulation of the polymer cylinders and a geometric non linear analysis (GNA) is used for the polymer cylinders. In Fig. 18 the load displacement curves of one experiment is compared to the results of GNAs with the same geometry. For the experiment the stiffness of the machine is taken into account. For the Young's modulus of the simulations, the mean Young's modulus and the mean Young's modulus plus and minus the standard deviation was considered. The stiffness of the experiments is within the range of the GNAs.

The steel cylinders however were observed to buckle plastically. Consequently, the plastic behavior was considered in the numerical analyses by utilizing a material model including isotropic plasticity based on the yield stress gathered from coupon tests. Hence, the simulations were set up as load-controlled geometrically and materially non linear analysis (GMNA).

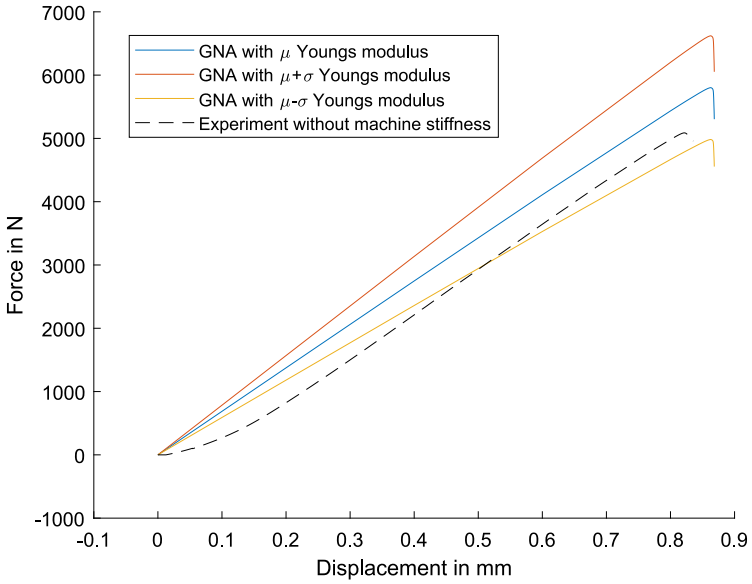

Fig. 18. Load displacement curve of one experiment and GNAs with the measured geometry and mean, mean plus standard deviation and mean minus standard deviation of the Young's modulus.

Table 8
Mean values and standard deviation of λ of MC.

Eccentricity	Mean value λ	Standard deviation λ
0 mm	0.7444	0.1378
5 mm	0.7154	0.1266
10 mm	0.7229	0.1275
15 mm	0.7234	0.1277
20 mm	0.7277	0.1308
40 mm	0.7367	0.1333

Table 9
Mean values and standard deviation of λ of experiment.

Eccentricity	Mean value λ	Standard deviation λ
0 mm	0.7152	0.1318
5 mm	0.7590	0.1251
10 mm	0.7649	0.1356
15 mm	0.7697	0.1269
20 mm	0.7781	0.1287
40 mm	0.7463	0.1264

6.3. Monte Carlo simulation of the polymer cylinders

To analyze buckling of the polymer cylinders numerically, several Monte Carlo (MC) simulations were performed. For the MC simulation 200 random parameters were generated and for each realization every load case of the experiment (eccentricity of 0 mm, 5 mm, 10 mm, 15 mm, 20 mm, 40 mm) was considered. To calculate the buckling loads, a geometrically non-linear Finite Element analysis was used. The geometric imperfections, the nodal thickness and the Young's modulus of the cylinder were considered as random parameters. The random geometric imperfection of the nodes was generated from the measured cylinder geometry, as well as the thickness on each node. The material property, namely the Young's modulus, was also considered random, because the scatter of the material parameter was found to be large for the 3D printed specimens.

Another MC with all random parameters (geometric imperfection, thickness and Young's modulus) was performed. The results of that MC simulation are compared to the experiment in Fig. 20. The Table 10 shows the mean values and standard deviation of the buckling loads and moments from the MC simulation. With the MC simulation, the mean value of λ is slightly lower for the eccentricity with the exception of 0 mm eccentricity. The standard deviation is slightly higher with the exception of 10 mm eccentricity compared to the experiment (see Tables 8 and 9). The cumulative distribution functions (CDF) and the probability density functions (PDF) of λ for the eccentricity of 40 mm of the MC simulation and the experiment are compared in Fig. 19. The CDFs of all eccentricities are given in Appendix A.1.

The MC simulation show a similar scatter of the normalized load factor to the experiment. However, the results of the MC scatter nearly on a line, meaning that the ratio of buckling load and buckling moment does not change much within one load case. The experiments show a different behavior. The scatter of the ratio of buckling moment and buckling load is much higher. This effect could not be reproduced with different imperfections taken into account (e.g. imperfect load introduction). One potential reason is the cross talking of the load cell, i.e. a signal for the recorded bending moment originating from axial load. Calibration reports of the load cell estimate the cross talking in a range of 2 Nm, which does not fully explain the observed scatter.

To investigate which random parameters influence the buckling of the cylinders, different sets of random parameters were used. The results for considering only geometric imperfection as random are shown in Fig. 21 on the left and for thickness imperfection in Fig. 21 on the right. The scatter of the results for geometric imperfection is much lower compared to the simulation with only random thickness. The thickness of the polymer cylinder influences the buckling more than the geometric imperfections. The mean values of the buckling loads and moments are smaller, if the random thickness is used in the simulation. A closer look at the thickness measurements reveals that the mean value of the measured thicknesses of four cylinders is bigger than the initial thickness of 1 mm, while the other 18 cylinders have a mean thickness below 1 mm. In addition to that, the highest mean value is with 1.021 mm only 2,11% bigger than the initial thickness, and the lowest mean value for the thickness is with 0.855 mm more than 14% smaller than the initial thickness. In conclusion, a randomly generated thickness results in an average thickness below the initial thickness, which reduces the buckling load and moment. This can be observed by comparing the two MC simulations with different sets of random parameters. Comparing the normalized load factor λ shows that the mean and the standard deviation of λ is higher for the MC with random geometric imperfections compared to the MC with random thickness. In other words, the thickness deviations have a stronger influence on the buckling load distribution that the geometric imperfections. This is also

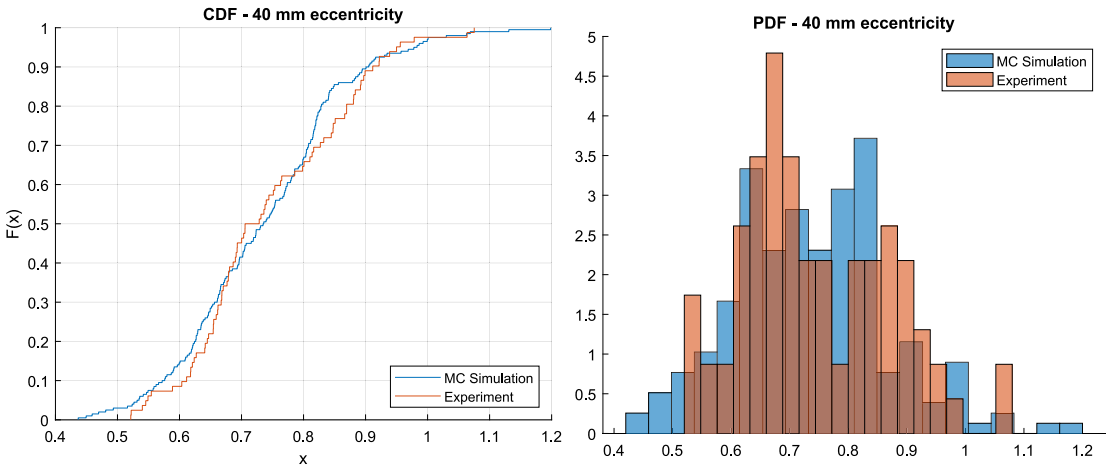

Fig. 19. CDF (left) and PDF (left) of λ for 40 mm eccentricity for the MC simulation and experiment compared.

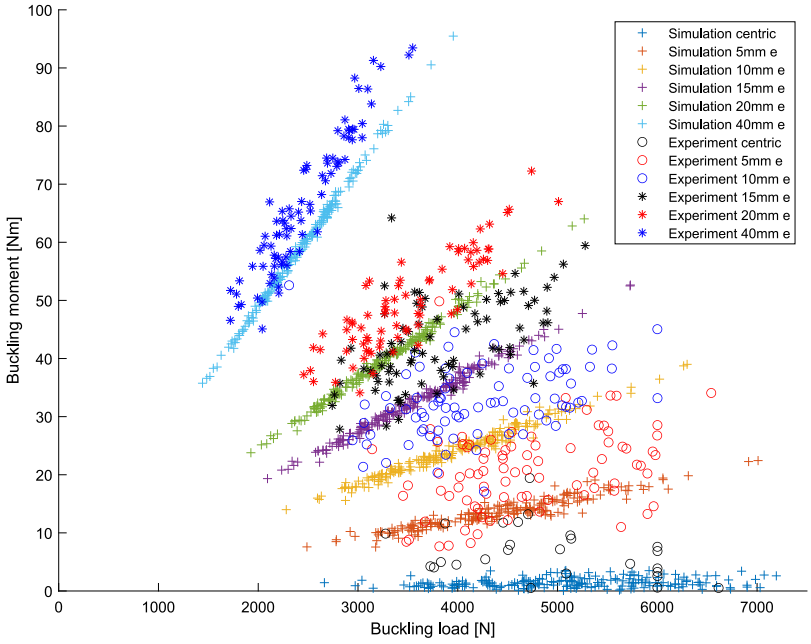

Fig. 20. Experimental results and Monte Carlo results.

Table 10
Mean values and standard deviation of the buckling load and buckling moment of the MC simulation with random geometric imperfections, thickness and Young's modulus.

Eccentricity	Mean value Buckling moment	Standard deviation Buckling moment	Mean value Buckling load	Standard deviation Buckling load
0 mm	1.43 Nm	0.80 Nm	5112 N	946 N
5 mm	13.54 Nm	2.62 Nm	4422 N	783 N
10 mm	24.26 Nm	4.35 Nm	3991 N	704 N
15 mm	32.78 Nm	5.79 Nm	3598 N	635 N
20 mm	39.95 Nm	7.13 Nm	3290 N	591 N
40 mm	59.10 Nm	10.53 Nm	2431 N	440 N

observed when plotting the evolution of the stochastic moments over the eccentricity, which is shown in Fig. 22. The graph also depicts that for the polymer cylinders considered, the eccentricity and hence, the combination of bending moment and axial force, has a negligible influence on the first stochastic moments. This finding cannot easily be generalized, especially since the cylinders considered have a very small slenderness (R/t) which yields a smaller sensitivity to geometric imperfections. Furthermore, the introduction of bending through an eccentricity limits the region in which the load combination could be tested.

7. Conclusion

In testing 22 polymer and seven steel shells, the present work provides the largest experimental test series of axially compressed cylinders since the test campaign conducted at the TU Delft using beer cans [29]. Particularly the systematic experimental investigation of combined axial compression and bending presents represents a significant expansion of the data base of multiaxial shell buckling tests. Since the polymer cylinders buckled elastically, the same set of cylinders was

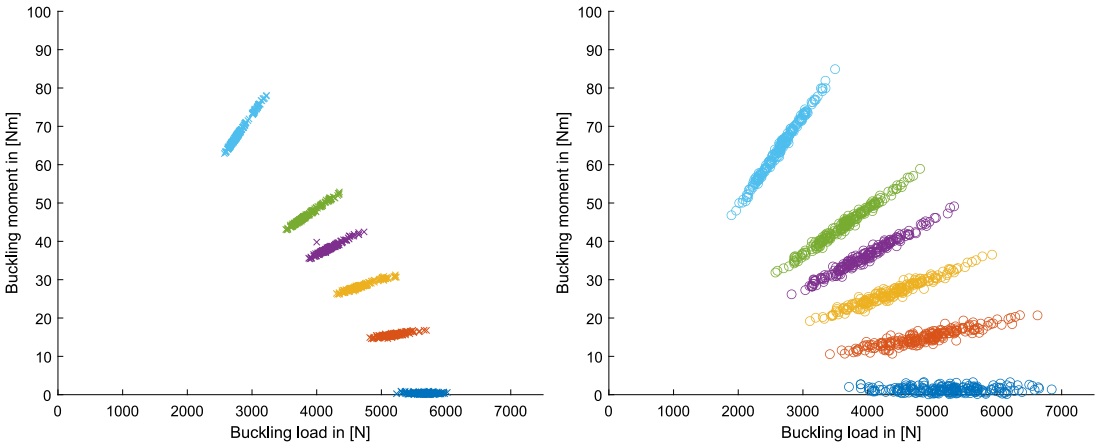

Fig. 21. Results of MC simulation with 200 realization of random geometric imperfection (left) and random thickness (right).

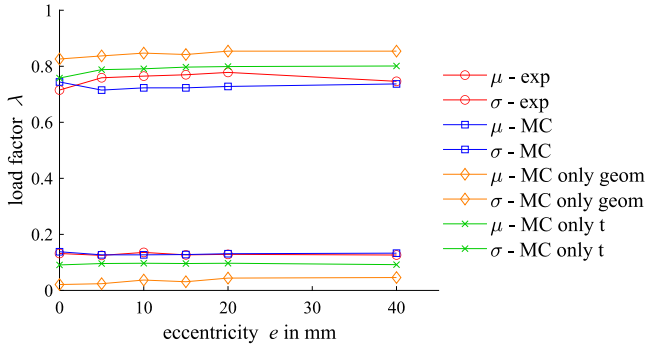

Fig. 22. Mean values and standard deviations of experimental results and MC simulation results with different random parameters as load factor over eccentricity.

used for tests under multiple combinations of axial force and bending moment. The steel cylinders on the other hand buckled and deformed plastically and therefore were each tested once with the same target load ratio of compression and bending. A normalized load factor was introduced and it could be shown to allow comparing results from different experiments and even test series with combined loading.

The larger test series with polymer shells allowed for the first time to experimentally determine the stochastic distribution of buckling load for various combined load cases. The probabilistic numerical model was validated on the test data and through Monte Carlo simulations and therefore allowed to quantify the effect of different sources of uncertainty. For the polymer cylinders, the deviations of thickness have stronger influence on the distribution of buckling load than the geometric imperfections, compared to the steel cylinders and other test series. The reason is the low slenderness of the polymer cylinders considered. Hence, the findings of the present studies are strictly limited to cylinders with low slenderness. Furthermore, only unstiffened isotropic cylinders are considered and no other load combinations than axial compression and bending have been investigated. Therefore, future studies will be carried out focusing on cylinders with higher slenderness and other load combinations (e.g. torsion and axial compression). Furthermore, with regards to lightweight design and applications, the buckling of cylindrical shells made from anisotropic materials in multiaxial load cases should be investigated.

CRediT authorship contribution statement

Niklas Reuter: Writing – review & editing, Writing – original draft, Visualization, Investigation. **Stefan Panek:** Writing – review & editing, Writing – original draft, Investigation. **Benedikt Kriegesmann:** Writing – review & editing, Writing – original draft, Supervision, Project administration, Methodology, Funding acquisition, Conceptualization. **Georgios Balokas:** Writing – review & editing, Investigation, Conceptualization. **Tobias S. Hartwich:** Writing – review & editing, Investigation, Conceptualization. **Dieter Krause:** Writing – review & editing, Supervision, Funding acquisition, Conceptualization.

Declaration of competing interest

The authors declare that they have no known competing financial interests or personal relationships that could have appeared to influence the work reported in this paper.

Data availability

The geometric and thickness imperfections of the 22 polymer cylinders and the buckling loads of the experiment are available under https://doi.org/10.15480/882.13221.

Acknowledgments

This research was funded by the German Research Foundation (Deutsche Forschungsgemeinschaft, DFG) via project No. 463883313. The statements in this contribution do not necessarily represent the opinion of the DFG.

Appendix

A.1. CDF plots of λ of the MC simulation and experiment

See Fig. 23.

A.2. Measured geometric imperfections

Figs. 25 and 24 show the scaled measured geometric imperfections of the polymer cylinders. The Fourier coefficients of the measured cylinder geometries and thickness are published via the TUHH open access repository TORE under the link https://doi.org/10.15480/882.13221. The notation of the cylinders indicate the name of the used printer (C and S) and the date of print.

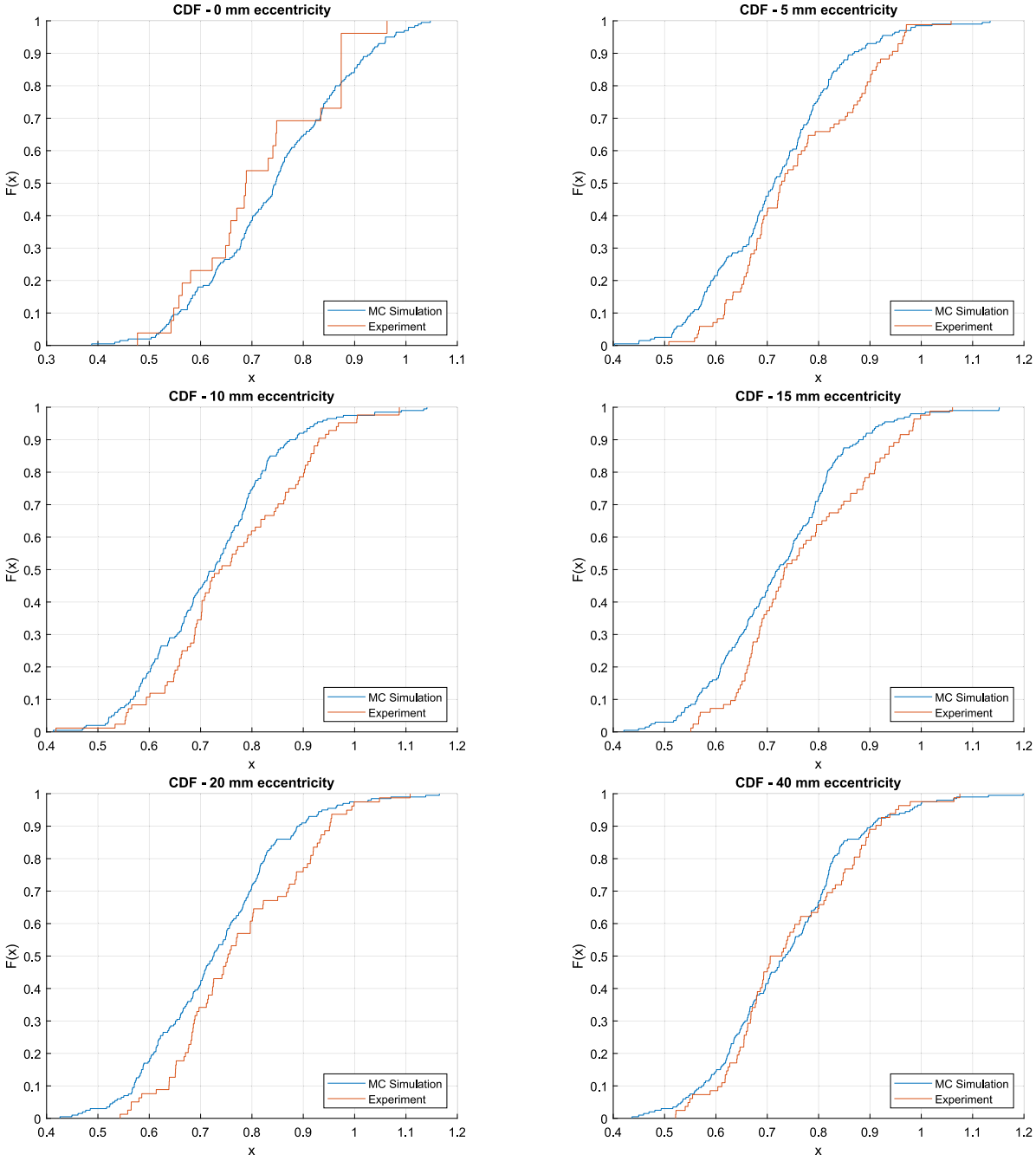

Fig. 23. CDF plots of λ of the results of the MC simulation with geometric, thickness and material imperfections compared to the results of the experiment for every eccentricity.

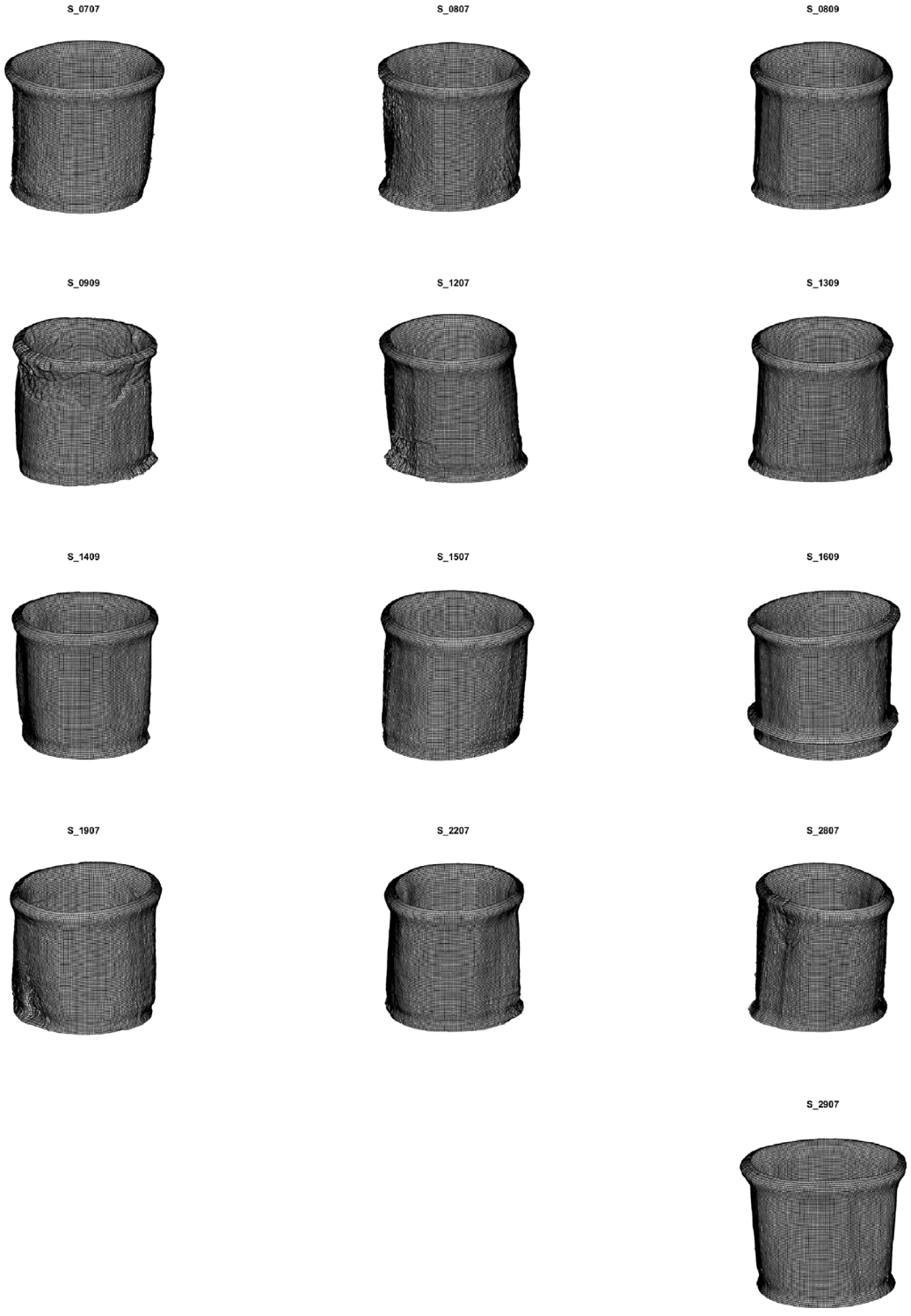

Fig. 24. Measured polymer cylinders from printer S.

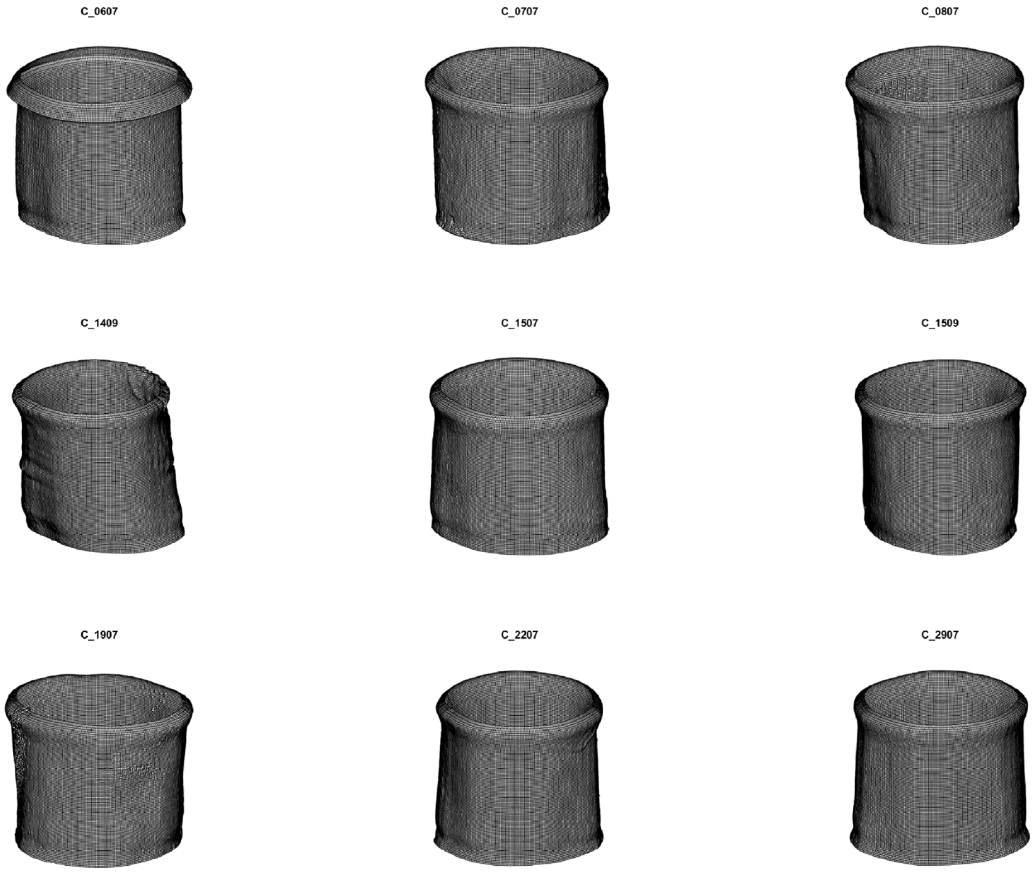

Fig. 25. Measured polymer cylinders from printer C.

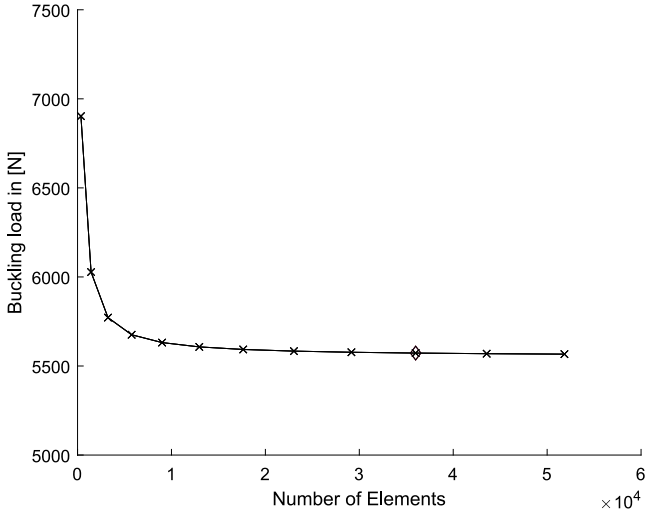

Fig. 26. Convergence study of an imperfect polymer cylinder with a centric loading, the used mesh is indicated with the diamond.

A.3. Mesh convergence

To validate the mesh of the FE analyses, a mesh convergence study was performed for geometrical non-linear FE analysis of a centric load case of an imperfect polymer cylinder. The result of this study is shown in Fig. 26. The result indicates, that the chosen mesh with 36360 elements is sufficient.

References

[1] M.W. Hilburger, Buckling of Thin-Walled Circular Cylinders, NASA SP-8007/REV2, NASA, 2020.
[2] J. Singer, T. Weller, J. Arbocz, Buckling Experiments: Experimental Methods in Buckling of Thin-Walled Structures, Vol. 1, Wiley, New York, 1997.
[3] J. Singer, T. Weller, J. Arbocz, Buckling Experiments: Experimental Methods in Buckling of Thin-Walled Structures, Vol. 2, John Wiley & Sons, Inc., Hoboken, NJ, USA, 2002.
[4] J. Arbocz, Past, present and future of shell stability analysis, Z. Flugwiss. Weltraumforsch. 5 (6) (1981) 335–348.
[5] I. Elishakoff, Uncertain buckling: Its past, present and future, Int. J. Solids Struct. 37 (46–47) (2000) 6869–6889, http://dx.doi.org/10.1016/S0020-7683(99)00318-2.
[6] T.A. Winterstetter, H. Schmidt, Stability of circular cylindrical steel shells under combined loading, Thin-Walled Struct. 40 (10) (2002) 893–910, http://dx.doi.org/10.1016/S0263-8231(02)00006-X.
[7] J. Hutchinson, Axial buckling of pressurized imperfect cylindrical shells, AIAA J. 3 (8) (1965) 1461–1466.
[8] H.-S. Shen, P. Zhou, T.-Y. Chen, Postbuckling analysis of stiffened cylindrical shells under combined external pressure and axial compression, Thin-Walled Struct. 15 (1) (1993) 43–63, http://dx.doi.org/10.1016/0263-8231(93)90012-Y.
[9] H.-S. Shen, Postbuckling of shear deformable cross-ply laminated cylindrical shells under combined external pressure and axial compression, Int. J. Mech. Sci. 43 (11) (2001) 2493–2523, http://dx.doi.org/10.1016/S0020-7403(01)00058-3.
[10] H. Abramovich, J. Singer, T. Weller, Repeated buckling and its influence on the geometrical imperfections of stiffened cylindrical shells under combined loading, Int. J. Non-Linear Mech. 37 (4–5) (2002) 577–588, http://dx.doi.org/10.1016/S0020-7462(01)00085-3.
[11] F. Bridget, C. Jerome, A. Vosseller, Some new experiments on buckling of thin-wall construction, Trans. Am. Soc. Mech. Eng. 56 (6) (1934) 569–578.
[12] E.F. Bruhn, J. Kempner, Tests on Thin-Walled Celluloid Cylinders to Determine the Interaction Curves Under Combined Bending, Torsion, and Compression or Tension Loads, NACA TN-951, National Advisory Committee for Aeronautics, 1945.
[13] C.T. Herakovich, Theoretical-Experimental Correlation for Buckling of Composite Cylinders Under Combined Compression and Torsion, NASA CR-157358, 1978.

[14] H.-R. Meyer-Piening, M. Farshad, B. Geier, R. Zimmermann, Buckling loads of CFRP composite cylinders under combined axial and torsion loading–experiments and computations, Compos. Struct. 53 (4) (2001) 427–435.
[15] C. Bisagni, P. Cordisco, An experimental investigation into the buckling and post-buckling of CFRP shells under combined axial and torsion loading, Compos. Struct. 60 (4) (2003) 391–402, http://dx.doi.org/10.1016/S0263-8223(03)00024-2.
[16] H. Otsuka, T. Koga, Buckling of circular cylindrical shells under beam-like bending. 1st report. Experiment, J. Japan Soc. Aeronaut. Space Sci. 43 (1995).
[17] T. Ghanbari Ghazijahani, H. Showkati, Bending experiments on thin cylindrical shells, in: Materials with Complex Behaviour II: Properties, Non-Classical Materials and New Technologies, Springer, 2012, pp. 119–139.
[18] General Rules: Strength and Stability of Shell Structures, Eurocode 3 Part 1.6, Brussels, Belgium, 2002.
[19] S. Drücker, J.K. Lüdeker, M. Blecken, A. Kurt, K. Betz, B. Kriegesmann, B. Fiedler, Probabilistic analysis of additively manufactured polymer lattice structures, Mater. Des. 213 (2022) 110300, http://dx.doi.org/10.1016/j.matdes.2021.110300.
[20] B. Plaumann, O. Rasmussen, D. Krause, System analysis and synthesis for the dimensioning of variant lightweight cabin interior, in: 54th AIAA/ASME/ASCE/AHS/ASC Structures, Structural Dynamics, and Materials Conference, 2013, p. 1632, http://dx.doi.org/10.2514/6.2013-1632.
[21] T.S. Hartwich, S. Panek, D. Wilckens, M. Bock, D. Krause, The influence of the manufacturing process and test boundary conditions on the buckling load of thin-walled cylindrical CFRP shells, Compos. Struct. 308 (2023) 116674, http://dx.doi.org/10.1016/j.compstruct.2023.116674.
[22] C. Schillo, D. Röstermundt, D. Krause, Experimental and numerical study on the influence of imperfections on the buckling load of unstiffened CFRP shells, Compos. Struct. 131 (2015) 128–138, http://dx.doi.org/10.1016/j.compstruct.2015.04.032.
[23] J. Arbocz, H. Abramovich, The Initial Imperfection Data Bank at the Delft University of Technology: Part I, Tech. Rep. LR-290, TU Delft, LR-290, 1979.
[24] B. Kriegesmann, R. Rolfes, C. Hühne, A. Kling, Fast probabilistic design procedure for axially compressed composite cylinders, Compos. Struct. 93 (2011) 3140–3149, http://dx.doi.org/10.1016/j.compstruct.2011.06.017.
[25] C. Schillo, B. Kriegesmann, D. Krause, Reliability based calibration of safety factors for unstiffened cylindrical composite shells, Compos. Struct. 168 (2017) 798–812, http://dx.doi.org/10.1016/j.compstruct.2017.02.082.
[26] S. Panek, T.S. Hartwich, D. Krause, Directional effects of load deviations on the buckling of cylindrical shells in experiment and design, in: DS 119: Proceedings of the 33rd Symposium Design for X (DFX2022), 2022, http://dx.doi.org/10.35199/dfx2022.03.
[27] C. Hühne, R. Zimmermann, R. Rolfes, B. Geier, Sensitivities to geometrical and loading imperfections on buckling of composite cylindrical shells, in: Proceedings European Conference on Spacecraft Structures, Materials and Mechanical Testing, 11.-13. Dezember 2002, Toulouse, France, 2002.
[28] H.N.R. Wagner, C. Hühne, K. Rohwer, S. Niemann, M. Wiedemann, Stimulating the realistic worst case buckling scenario of axially compressed unstiffened cylindrical composite shells, Compos. Struct. 160 (2017) 1095–1104, http://dx.doi.org/10.1016/j.compstruct.2016.10.108.
[29] R. Dancy, D. Jacobs, The Initial Imperfection Data Bank at the Delft University of Technology: Part II, Tech. Rep. LR-559, Delft University of Technology, Faculty of Aerospace Engineering, 1988, URL http://resolver.tudelft.nl/uuid:9da23db8-dba9-4464-96cf-e733ee924019.